In vitro bioactivity of titanium/hydroxyapatite composites fabricated by powder metallurgy

Ye, Hezhou; Liu, Xing Yang; Hong, Han Ping

Publisher's version / Version de l'éditeur:

IMI Series, 2009

In vitro bioactivity of Titanium/hydroxyapatite composites fabricated by powder metallurgy

Hezhou Ye [a], Xing Yang Liu[b], Han Ping Hong [a]

[a] Faculty of Engineering, the University of Western Ontario, London, Ontario, N6A 5B8, Canada

[b] Industrial Materials Institute, National Research Council of Canada, London, Ontario, N6G 4X8, Canada

Corresponding author information:

Name: Hezhou Ye

Email: hye5@uwo.ca; hyeuwo@gmail.com

Telephone: 1-519-430-7139

Fax: 1-519-430-7064

Abstract

Titanium/hydroxyapatite (Ti/HA) composites with low HA additions (≤ 20 vol.%) were fabricated by powder metallurgy and the *in vitro* bioactivity of the composites was evaluated in a simulated body fluid (SBF). After immersion in the SBF, all composite samples induced nucleation and growth of carbonated apatite. With the increase of the HA addition, co-precipitation of $CaCO_3$ and $Mg(OH)_2$ with the apatite was detected on the composite surface at an early stage of immersion. The *in vitro* behaviour of the composites and the precipitates formed during immersion were determined by both the surface conditions and the chemistry of the composite. The results indicated that the Ti/HA composites with low HA addition were bioactive and had the potential to be used for hard-tissue replacement.

Keyword: Titanium, Hydroxyapatite, composites, in vitro

1 Introduction

Among various materials developed as bone substitutes, hydroxyapatite (HA, $Ca_{10}(PO_4)_6(OH)_2$) has attracted intensive interest due to its close resemblance of the chemical structure to that of the bones and teeth [1]. It has excellent biocompatibility and can integrate into surrounding tissues after implantation, supporting the bone ingrowth [2, 3]. However, the poor mechanical properties of HA as compared to the natural bones, especially the low tensile strength and fracture toughness, significantly restrict its direct applications as load-bearing implants [4].

Due to their superior mechanical properties and good biocompatibility, Ti and Ti alloys are widely used for load-bearing implant applications [5]. These materials, however, are generally bioinert and can not promote tissue bonding to the implants, which may cause the metal implant loose or even separation from surrounding tissues in the long term [6]. Bioactive fixation, using the growth of newly formed bone to bond the implant with the surrounding tissues, is an ideal solution for overcoming the drawbacks of the Ti implants. Coating Ti substrate with HA is a common method used to improve the bioactivity of the implant and various coating techniques have been developed [7-9]. Due to the different physical, chemical and mechanical properties between the coating material and the substrate, the bonding strength is low and cracks are easy to form at the interface, which can lead to separation of the coating and the formation of ceramic debris which can disturb the proliferation and osteocalcin synthesis of human osteoblasts [10].

Fabrication of Ti/HA composites by powder metallurgy can circumvent the inherent disadvantages of the coating methods [11]. It has been confirmed that the Ti/HA composites with over 20 vol.% HA addition were biocompatible and bioactive both *in vitro* and *in vivo* [11-17]. Because the mechanical properties, especially the bending strength and fracture toughness, decrease markedly with the rise of HA addition, a bioactive composite with a lower concentration of HA is desirable for hard tissue implant applications [17]. Although the *in vitro* behaviours of some Ti/HA composites have been reported, the bioactivity of the composite with low HA addition is lacking and the apatite formation mechanism of the Ti/HA composite in the simulated body fluid (SBF) is still far from conclusive [11, 16].

In the present work, Ti/HA composites with different HA additions were fabricated by a powder metallurgy method and the bioactivity of the composite was evaluated in a simulated body fluid (SBF). Factors contributing to the *in vitro* behaviour of the Ti/HA composites were discussed.

2 Experimental procedures

2.1 Preparation of the composites

Commercially pure (CP) titanium powder (Atlantic Equipment Engineers, USA) and HA powder (Pentax, Japan) were used as the starting materials. Ti/HA powder mixtures with 5, 10 and 20 vol.% HA were sealed in glass vials under argon atmosphere and mixed using a 3D mixer (Laval Lab, Canada) for 48 hrs. The blended mixtures were subsequently compacted uniaxially in a rigid die under a pressure of 350 MPa and then sintered at 1200 ^{o}C for 1 hr in argon. For convenience, the composite sample was denoted as TiXHA, where X refers to the volume percentage of HA.

2.2 *In vitro* test in the simulated body fluid

To evaluate the bioactivity of the composite, the SBF solution was prepared using Kokubo's formulation [18]. The inorganic ion concentrations in the SBF are nearly equal to those in human blood plasma, as shown in Table 1. Appropriate amounts of the reagents were dissolved in deionised water following the order listed in Table 2. The pH value of the solution was finally buffered to 7.4 at 37 ^{o}C with hydrochloric acid (HCl) and tris-hydroxymethyl aminomethane (Tris). Because the SBF can be easily contaminated by bacteria even after short time exposure to the ambient environment, 1g/l

NaN_3 was added to the solution to inhibit the growth of the anaerobic bacteria and maintain the ion concentrations in the solution [19].

Table 1 *Inorganic ion concentrations in the simulated body fluid (SBF) and the human blood plasma (mM)*

Table 2 *Purity and amount of the reagents for preparing 1000 ml of the SBF solution*

The as-sintered composite samples were polished with sandpaper up to 1200 grit and then washed ultrasonically in acetone, ethanol and deionised water for 10 min each. The cleaned samples were dried by a heat gun and subsequently immersed into the SBF. After soaking for various periods of time, the samples were removed from the fluid, gently rinsed with deionised water and naturally dried in a fume hood. The SBF was not refreshed throughout the period of immersion.

2.3 Characterizations

The phases in the sintered samples were identified by X-ray diffraction (XRD, Philip X'Pert, Netherlands) with a Cu target at 40 kV and 40 mA. The surface condition of the composite before soaking into the SBF was characterized using X-ray photoelectron spectroscopy (XPS, Kratos Axis Ultra, USA) with a monochromatic Al Kα source. Spectra were processed with CasaXPS software (version 2.2.107).

The surface morphology of the samples was observed by a scanning electron microscope (SEM, Hitachi E3500, Japan) with an energy-dispersive X-ray analyzer (EDX) attachment. The composite surface after soaking in SBF were examined by low-angle XRD at a glancing angle of 1° with a scanning speed of 0.02 °/s. The chemical

structure of the precipitates was identified using Fourier transform infrared spectroscopy (FTIR, Tensor 27, Bruker, USA). The pH value of the SBF was measured with a pH meter (Accumet, Fisher, USA) and ion concentrations in the fluid were determined by an inductively coupled plasma atomic emission spectroscopy (ICP-AES, Perkin-Elmer, USA).

3 Results

3.1 Phases in the sintered composites

Fig.1 shows the XRD patterns of the composites before and after sintering. For the as-compacted samples, the peaks assigned to Ti (JCPDS 44-1294) dominated the patterns and HA peaks become recognizable as the HA addition increased in the composite. After sintering at 1200 ^{0}C, the predominant peaks in the patterns were still from Ti and a number of week peaks were observed, while the original HA peaks disappeared even in the pattern of Ti20HA. The relative intensities of the new peaks increased with the HA addition in the composite. The position of the peaks matched that of CaO and titanium phosphides, which also agreed with the reported results [11, 19]. Due to the very low intensity of the peaks and the complexity of Ti phosphides, it was difficult to definitely determine the exact composition of the Ti phosphide phase in the composite [20].

Fig. 1 *XRD patterns of the composites (a) before and (b) after sintering at 1200 ^{o}C*

3.2 Surface characterization of the composite

The survey and high resolution XPS spectra for the TiXHA samples (X≤20) were shown in Fig. 2. As detected by the survey scan, the dominant elements on the composite surfaces were Ti, Ca, C and O. The relatively strong C signal was most likely due to surface contamination by adsorbed organic molecules, which is normally observed for surfaces exposed to air [21]. No P was present on the surface of Ti5HA or Ti10HA, while only trace of P was detected on Ti20HA surface. Furthermore, with the increase of HA addition in the composite, Ca peaks were intensified in the survey spectrum and the Ti peaks were weakened, indicating that more Ca was present on the surface.

Fig. 2 *The XPS survey and high resolution spectra of the composite surfaces (a1-a4) Ti5HA; (b1-b4) Ti10HA; (c1-c4) Ti20HA*

In order to identify the valence states of the elements, high-resolution narrow scans were conducted for the key elements and the obtained spectra were deconvoluted. For all composites, the Ti 2p spectra were similar in shape and they were decomposed into complex structure, which could be ascribed to the presence of different Ti phases. Two major subpeaks located at the binding energies of 464.7 eV and 458.9 eV were attributed to 2p1/2 and 2p3/2 peaks of Ti^{4+}, indicating that Ti was mainly presented as TiO_2 on the surface [22]. Another dominant peak appeared at the binding energy of 453.7eV was attributed to the 2p3/2 state of Ti metal [23]. In addition, the 2p doublet of Ti^{3+} were resolved at binding energies of 463.3 eV and 457.7 eV, and the 2p bands of Ti^{2+} were displayed at the binding energies of 456 eV and 461.5 eV [24].

The O 1s spectrum could be deconvoluted into three individual peaks, representing the oxygen in oxide (O^{2-}), hydroxide (adsorbed OH^- group), and water (H_2O). The binding energies of the three statuses were about 530.5 eV, 531.5 eV and 532.5 eV, respectively [23, 25]. As shown in Fig. 2, with the increase of HA addition, the percentages of O 1s components due to chemisorbed water and oxides decreased distinctly, while the concentration of oxygen in OH^- increased significantly. For Ti5HA, the principal O1s component (40 at.%) was contributed by oxides and 26 at.% of O1s was due to adsorbed water. In contrast, the majority (over 70 at.%) of the oxygen on Ti10HA or Ti20HA surface was originated from OH^- group and the O 1s peak due to water content was invisible in the O 1s spectrum of Ti20HA.

The high resolution Ca 2p spectra obtained from the composite surfaces were quite consistent. The spin orbit splitting was kept at 3.6 eV and both Ca 2p1/2 and 2p3/2 bands were symmetrical, indicating that Ca existed as divalent ion [26]. Due to the insensitivity of the Ca 2p spectra to the chemical environment, the observed Ca 2p3/2 spectra fall into the binding energy ranges of various Ca phases, such as $CaTiO_3$, CaO and $CaCO_3$ [27, 28]. It was noted that the full width at half maximum (FWHM) of the Ca 2p3/2 was increased from 1.54 eV to 2.89 eV as the HA addition increased from 5 vol.% to 20 vol.%. These facts implied that the Ca on the composite surface might exist in two or more distinct phases.

3.3 Surface morphologies of the composite after immersion into SBF

The surface morphologies of Ti5HA during soaking in the SBF for various periods were shown in Fig. 3. Before immersion, the composite surface was featured by

uniformly distributed polished grooves and few micro-scale pores. After 8 hr immersion in the SBF, no significant change occurred on the composite surface, except for the appearance of some dispersed tiny globular particles. With the increase in soaking time, more and more globular particles deposited on the surface and most of the surface area was colonized by the particles after 7 day immersion in the SBF. Further increase of the immersion time did not lead to significant change of the surface morphology.

Fig. 3 *Surface morphologies of the sintered Ti5HA after soaking in the SBF: (a) 0 h, (b) 8 h; (c) 1 day; (d) 3 days; (e) 7 days; (f) 14 days*

Fig. 4 shows the surface morphologies of Ti10HA before and after soaking into the SBF. Before soaking, the composite surface contained many open pores. However, after immersion in the SBF for 8 hrs, most of the pores were filled by the newly-formed deposition and the surface became smooth. With the elongation of the immersion time, the precipitate became denser and thicker and the whole surface of the composite was covered by the coating after 1 day. 1 week later, a uniform layer of precipitation formed on the composite surface and the morphology was no long changed with further elongation of the soaking time.

Fig. 4 *Surface morphologies of the sintered Ti10 HA after soaking in the SBF: (a) 0 h, (b) 8 h; (c) 1 day; (d) 3 days; (e) 7 days; (f) 14 days*

The SEM micrographs of Ti20HA surface before and after immersion in the SBF were shown in Fig. 5. The composite surface was highly porous before immersion. After 8 hr soaking in the SBF, many globular grains and regular polygonal particles were deposited on the surface. Some pores on the surface were filled by the precipitates after 1 day immersion and more tiny polygonal grains formed on the composite surface. After 3 days, the whole Ti20HA surface was fully covered by the precipitates and no polygonal phases were observed. The formed precipitates were inter-linked spheres instead of polygons, as shown in high magnification micrograph of inset. With the increase of soaking time, more dense coating was developed.

Fig. 5 *Surface morphologies of the sintered Ti20HA after soaking in the SBF: (a) 0 h, (b) 8 h; (c) 1 day; (d) 3 days; (e) 7 days; (f) 14 days*

Fig. 6 shows a high magnification SEM micrograph of the surface after 1 day immersion, which displays the details of the precipitates on Ti20HA surface. Three distinct shapes were present in the precipitate, i.e., tiny spheres, flaky crystallines, and regular polygonal particles. The EDX patterns of the three phases indicate that the tiny spheres contained mainly Ca, P and O, and therefore were most likely apatite. The flaky phase was enriched with Mg and O, and the polygonal particle was mainly composed of Ca and O.

Fig. 6 *EDX analysis of the SEM morphological features on Ti20HA surface after 1 day immersion in the SBF*

3.4 Characterization of the precipitates formed on the composite surface

The FTIR spectra of the precipitate collected from the composite surface after immersed in the SBF for various periods are shown in Fig. 7. Because the precipitate amount formed on the Ti5HA surface after immersion in the SBF within 7 days was too low to be analyzed, only the precipitate formed on the surface after 14 day incubation was characterized by FTIR. All the spectra demonstrated very similar structure as the characteristic spectrum of carbonated apatite, which is regarded as bone resembling material [29]. The intense and broad bands at 3450 cm^{-1} and 1638 cm^{-1} were assigned to stretching and bending vibrations of OH^- group in water, respectively [30]. These characteristic bands were due to the hydroscopic feature of the precipitate and/or the absorbed moisture from atmosphere. In the spectrum, the predominant band in the range from 1100 to 950 cm^{-1} was attributed to the P-O symmetric stretching mode (v_3) of PO_4^{3-} group. Another strong peak, or doublet, at 600-500 cm^{-1} was due to the v_4 bending vibration of PO_4^{3-} [31]. At the same time, a broad band in the region from 1600 to1400 cm^{-1} and a sharp peak at 874 cm^{-1} were present in the spectrum, which were linked to the v_3 and v_2 vibration mode of CO_3^{2-} group [29]. Moreover, in the spectra of the precipitates after 14 day immersion in the SBF, a weak peak or a shoulder was observed at 469 cm^{-1}, assigned to the v_2 band of PO_4^{3-} in the carbonated apatite [30]. Therefore, all the precipitates coated on the composite surface during immersion in the SBF could be regarded mainly as bonelike carbonated apatite.

Fig. 7 FTIR of the precipitates formed on the composite surfaces after soaking in the SBF

There were some additional bands in the FTIR spectra of the precipitates formed on Ti10HA and Ti20HA surfaces. For Ti10HA, a shoulder at 711 cm^{-1} emerged in the spectra of the precipitates formed after 1 day, 3 day and 7 day immersion, which was assigned to the v_4 vibration of CO_3^{2-} in $CaCO_3$ [32]. However, it disappeared from the spectrum of the precipitate formed after 14 day immersion. For the 1 day formed precipitate on Ti20HA, the weak peak at 711 cm^{-1} appeared in the spectrum as well, indicating the presence of $CaCO_3$. On the high frequency side, a sharp band at 3692 cm^{-1} was located in the FTIR spectra of the precipitates formed after 1 day and 3 day immersion in the SBF, which was due to the stretching mode of OH^- in $Mg(OH)_2$ [33, 34].

Fig. 8 shows the low-angle XRD patterns of the composite surface during soaking in the SBF. With the elongation of the incubation time, the apatite peaks became stronger and the peaks from the substrate became weaker in the patterns. For Ti5HA, only the peaks due to apatite and the substrate were present in the XRD patterns (Fig. 8(a)). While for Ti10HA and Ti20HA, substantial peaks assigned to $CaCO_3$ appeared in the patterns at an early stage of immersion. However, after 2 weeks, the relative intensity of $CaCO_3$ peaks decreased and the apatite peaks became dominant in the XRD patterns of the precipitate coatings on the composite surfaces.

Fig. 8 Low-angle XRD patterns of the composite surface after immersion in SBF for various times: (a) Ti5HA; (b) Ti10HA; (c) Ti20HA

3.5 Changes of the SBF solution during the immersion of the composites

Fig. 9 shows changes in the pH value of the SBF and ion concentrations in the fluid during the immersion of the composites. For the same period of immersion, the SBF containing the composite with a higher HA addition generally had a higher pH value and calcium concentration, but a lower P concentration. The change of the pH value of the solutions over time demonstrated similar change tendency for samples with different concentrations of HA. It increased to a maximum at first and then dropped to a certain level, after which only slight change occurred with further increase in the immersion time. For the SBF containing Ti5HA, the pH value was relatively stable and it only fluctuated within 0.1. With the increase of HA addition, the change of the pH value after the composite immersion became more significant. After 3 days, the pH values of the SBF containing Ti10HA and Ti20HA increased from the original 7.40 to 7.80 and 8.33, respectively. Both of them dropped after 7 day immersion and then remained fairly constant. The change of the Ca concentration in the fluid containing Ti5HA was very different from others. After the immersion of Ti5HA in the SBF, the calcium concentration decreased rapidly at the beginning and then stabilized after 1 week. In contrast, the Ca concentration in the fluid containing Ti10HA or Ti20HA samples increased rapidly within the first day and then decreased with the elongation of immersion time. However, the P concentrations in all the solutions followed the same trend: declined quickly at first and then decreased slowly over time.

Fig. 9 pH value and ion concentrations in the SBF solution after the immersion the composites

4 Discussion

It is known that Ti promotes decomposition of HA during sintering, resulting in various reaction products under different conditions [11, 12, 35]. The current work confirmed that in the Ti/HA composites containing up to 20 vol.% of HA, HA had already completely decomposed during sintering at 1200 °C. In the sintered composite, Ti was still the primary crystal phase and the formation of CaO and Ti phosphides were detected, which agreed with the observation given in Ning [11].

FTIR and XRD characterizations of the samples immersed in the SBF showed that the TiHA composites could induce the formation of bone-like apatite in the SBF (Figs 6 and 7). Ning [12, 13] suggested that a key factor attributing to the bioactivity of the Ti50HA was hydration of Ti_2O, which could induce the apatite formation by the functional groups of the Ti-OH. It is widely accepted that the biological response to the implant will be determined by the microscopic (atomic level) surface properties of the materials and the tissue response is a result of the short range (<1 nm) interactions between the surface groups and the biological surroundings [36, 37]. Therefore, the bioactivity of the material is more associated with the functional groups within the outmost surface [38]. High resolution XPS spectra demonstrated that Ti existed in multiple valance status on the surface, including Ti^{2+}, Ti^{3+}, Ti^{4+} and Ti metal, differing from the Ti^{4+} condition corresponding to the natural Ti_2O oxide. The complex status of Ti was due to the oxygen

diffusion from the exterior surface to the inside during sintering, which was confirmed by XRD detection (Fig.1). The Ti suboxides are believed to be more active than TiO_2 in the physiological environment and represent a range of possibilities regarding, for instance, chemical bond coordination between the implant surface and adjacent biomolecules [39]. In the SBF, the Ti suboxides can be hydrated to form Ti-OH groups on the composite surface in the SBF following the equation:

$$2Ti_xO + xH_2O \rightarrow 2xTi - OH \quad (1)$$

The formed Ti-OH groups could incorporate calcium and then attract the phosphate and carbonate ions in the SBF by electrostatic potential interactions [40].. On the other hand, the Ca present on the composite surface could act as nuclei and lead to effective initial deposition of apatite from the solution [41]. Moreover, CaO in the sintered composite could react with water in the SBF according to:

$$CaO + H_2O \rightarrow Ca^{2+} + OH^- \quad (2)$$

The Ca^{2+} released from the composite according to Eq. (2) will enhance the supersaturation of Ca in the vicinity of the surface, and promote the nucleation and growth of the apatite. On the other hand, the reaction in Eq. (2) will lead to increase in the pH value of the SBF which was kinetically favourable for the formation of apatite from the SBF [42]. It can be expected that a higher concentration of HA in the composite, will lead to a higher Ca concentration and pH value in the fluid (Fig. 9). Once the apatite nuclei are formed, they can grow spontaneously by assembling the calcium, phosphate, and carbonate ions in the SBF.

After the immersion of Ti10HA and Ti20HA in the SBF, $CaCO_3$ was also detected in the precipitate on the surface of the composite at an early stage by both FTIR and XRD.

The formation of $CaCO_3$ formed both in *in vitro* and *in vivo* has also been observed by previous studies [33, 43]. The precipitation of $CaCO_3$ was related to the high concentrations of calcium induced by the reaction according to Eq. (2). After consuming the local HPO_4^{2-} for the apatite formation, the remaining Ca would react with HCO_3^-:

$$Ca^{2+} + 2HCO_3^- \rightarrow CaCO_3 + CO_2 + H_2O \quad (3)$$

With the increase of HA addition in the composite, the formation of $CaCO_3$ particles with regular polygonal geometry was more significant at the early stage of immersion, as shown in Fig.5.

In addition to $CaCO_3$ and carbonated apatite, the formation of $Mg(OH)_2$ on the surface of Ti20HA sample after immersion in the SBF was also confirmed by FTIR and the EDX analyses (Figs. 6 and 8). Because Ti20HA contained more CaO than Ti5HA and Ti10HA, a high concentration of OH^- groups could be induced according to Eq. (2) after immersion in the SBF. Mg^{2+} in the SBF would combine with the OH^- groups to form $Mg(OH)_2$ deposit [44]. However, the $Mg(OH)_2$ is not stable. It would be corroded in the SBF where Cl^- ions was present, forming highly soluble $MgCl_2$ and hydrogen gas [45]. The process could be summarized as:

$$Mg^{2+} + OH^- \rightarrow Mg(OH)_2(s) \quad (4)$$

$$Mg(OH)_2(s) + Cl^- \rightarrow Mg^{2+} + Cl^- \quad (5)$$

Therefore, with the elongation of the immersion time, $Mg(OH)_2$ was dissolved in the SBF and the hydroxyl peak disappeared from FTIR spectra.

It should be noted that the $CaCO_3$ co-precipitated with carbonated apatite is recognised as biocompatible and it will not change the bioactive feature of the composites. Even it is not observed in the *in vitro* studies, the formation of $CaCO_3$ can occur in the *in vivo*

environment due to the higher HCO_3^- concentration in the body fluid when the implant releases a high amount of Ca.

5 Conclusions

The in vitro bioactivity of the Ti/HA composite with low HA addition fabricated by powder metallurgy was evaluated in a simulated body fluid. All the Ti/HA composites with HA concentration varying from 5-20 vol.% could induce apatite nucleation and growth on its surface after immersion in the SBF, although higher HA concentration in the composites led to faster apatite deposition. Also, the co-precipitation of $CaCO_3$ and $Mg(OH)_2$ with carbonated HA was detected at an early stage in the composites with high concentration of HA, due to high Ca^{2+} and OH^- concentrations in the fluid released from the composites. The Ti-OH groups formed on the composite surface by the hydration of Ti oxides contributed to the bioactivity. Dissolution of CaO increased the pH value and Ca supersaturation of the SBF, which was kinetically favourable for the apatite nucleation and growth.

Acknowledgement

This research is supported by the Natural Science and Engineering Research Council of Canada. The help from David Arnold in XRD experiments, and Marco Zeman in SEM analysis are also gratefully acknowledged.

References

[1] K. Kato, H. Aoki, I. Tabota, M. Ogiso, Biomater. Med. Devices Artif. Organs. 7 (1979) 297.

[2] J.D. de Bruijn, C.A. van Blitterswijk, J. Davies, J. Biomed. Mater. Res. 29 (1995) 89.

[3] J. R. Woodard, A. J. Hilldore, S.K. Lan, C.J. Park, A.W. Morgan, et.al., Biomaterials. 28 (2007) 45.

[4] M. Jarcho, Clin. Orthop. Relat. Res. 157 (1981) 259.

[5] M.G. Shettlemore, K.J. Bundy, J. Biomed. Mater. Res. 45 (1999) 395.

[6] T. Albrektsson, H.A. Hansson, Biomaterials. 7 (1986) 201.

[7] D.G. Wang, Colloids Surf. B: Biointerfaces, 66 (2008) 155.

[8] M. Sygnatowicz, A. Tiwari, Mater. Sci. Eng. C, doi: 10.1016/j. msec.2008.06.036.

[9] G. Ciobanu, G. Carja, O. Ciobanu, Surf. Coat. Tech. 202 (2008) 2467.

[10] A.K. Roynesdal, E. Ambjornsen, H.R. Haanaes, Int. J. Oral Maxillofac. Implants. 14 (1999) 543.

[11] C.Q. Ning, Y. Zhou, Biomaterials, 23 (2002) 2909.

[12] C.Q. Ning, Y. Zhou, Acta Biomater. doi:10.1016/j.actbio.2008.04.015.

[13] C.Q. Ning, Y. Zhou, Biomaterials, 25 (2004) 3379.

[14] C.Q. Ning, Y. Zhou, H.L Wang, D.C. Jia, T.C. Lei, J. Mater. Sci. Lett. 19 (2000) 1243.

[15] C.L. Chu, X.Y. Xue, J.C. Zhu, Z.D. Yin, J. Mater. Sci. Mater. Med. 15 (2004) 665.

[16] C.L. Chu, X.Y. Xue, J.C. Zhu, Z.D. Yin, J. Mater. Sci. Mater. Med. 17 (2006) 245.

[17] C.L. Chu, J.C. Zhu, Z.D. Yin, S.D. Wang, Mater. Sci. Eng. A271 (1999) 95

[18] T. Kokubo, H. Takadama, Biomaterials, 27 (2006) 2907.

[19] F.J. Gil, A. Padros, J.M. Manero, C. Aparicio, M. Nilsson, J.A. Planell, Mater. Sci. Eng. C22 (2002) 53.

[20] H.Ye, X.Y. Liu, H. Hong, J. Mater. Sci. Mater. Med. doi:10.1007/s10856-008-3647-3.

[21] P. Babelon, A.S. Dequiedt, H. Mostefa-Sba, S. Bourgeois, P. Sibillot, M. Sacilotti, Thin Solid films, 322 (1998) 63.

[22] C. Combes, C. Rey, M. Freche, Colliods Surf. B: Biointerfaces, 11 (1998) 15.

[23] J. Xie, B.L. Luan, J. Biomed. Mater. Res., 84A (2008) 63.

[24] M.C. Biesinger, B.P. Payne, B.R. Hart, A.P. Grosvnor, N. S. McIntryre, L.W.M. Lau, R.C. Smart, J. Phy: Conf. Ser. 100 (2008) 012025, doi:10.1088/1742-6596/100/1/012025.

[25] X. Lu, Y. Wang, X.Yang, Q. Zhang, Z. Zhao, L. Weng, Y. Leng, J. Biomed. Mater. Res. 84A (2008) 523.

[26] M.T. Pham, H. Reuther, W. Matz, R. Mueller, J. Mater. Sci. Mater. Med. 11 (2000) 383.

[27] T.Hanawa, H. Ukai, K. Murakami, J. Electron Spectrosc. Relat. Pheonom. 63 (1993) 347.

[28] T. Hanawa, M. Ota, App. Surf. Sci. 55 (1992) 269.

[29] E. Landi, G. Gelotti, G. Logroscino, A. Tampieri, J. Europ. Ceram. Soc. 23 (2003) 2931.

[30] I. Rehman, W. Bonfield, J. Mater. Sci. Mater. Med. 8 (1997) 1.

[31] M.I. Zaki, H. Knozinger, B. Tesche, Langmuir. 22 (2006) 749.

[32] M. Mami, A. Lucas-Girot, H. Oudadesse, App. Surf. Sci. doi:101016/j.apsusc.2008.05.340

[33] N.J. Coleman, J.W. Nicholson, K. Awosanya, Cem. Con. Res. 37 (2007) 1518.

[34] R.A. Nyquist, R.O. Rageli, Handbook of infrared and Raman Spectra of Inorganic Compounds and Organic Salts, Vol.4: Infrared Spectra of Inorganic Compounds (3800-45 cm^{-1}) (Academic, San Diego, 1997), p. 235.

[35] J. Weng, X.G. Liu, X.D. Zhang, X.Y. Ji, J. Mater. Sci. Lett. 13 (1994) 159.

[36] A.G. Gristina, Science, 237 (1987) 1588.

[37] J. Lausmaa, B. Kasemo, App. Surf. Sci. 44 (1990) 133.

[38] X. Lu, Y. Wang, X.D. Yang, et.al., J. Biomed Mater Res. 84A (2008) 523.

[39] T. Albrktsson, H.A. Hansson, B. Kasemo, K. Larsson, I. Lundstrom, D. H. McQueen, R. Shalak, Ann. Biomed Eng. 11 (1983) 1.

[40] D. Wei, Y. Zhou, D. Jia, Y. Wang, Acta Biomater. 3 (2007) 817.

[41] E.V. Pecheva, L.D. Pramatarova, M. F. Maitz, M. T. Pham, A.V. Kondyuirin, App. Surf. Sci. 235 (2004) 176.

[42] X. Lu, Y. Leng, Biomaterials, 26 (2005) 1097.

[43] Y. Zhang, M. Mizuno, M. Yanagisawa, H. Takadama, J. Mater. Res. 18 (2003) 433.

[44] Y. Wang, M. Wei, J. Gao, J. Hu, Y. Zhang, Mater. Lett. 62 (2008) 2181.

[45] M.P. Staiger, A. M. Pietak, J. Huadmai, G. Dias, Biomaterials, 27 (2006) 1728.

Table 1 Inorganic ion concentrations in the simulated body fluid (SBF) and the human blood plasma (mM)

	Na^+	K^+	Ca^{2+}	Mg^{2+}	Cl^-	HCO_3^-	HPO_4^{2-}	SO_4^{2-}
Kokubo's SBF	142.0	5.0	2.5	1.5	147.8	4.2	1.0	0.5
Blood plasma	142.0	5.0	2.5	1.5	103.0	27.0	1.0	0.5

Table 2 Purity and amount of the reagents for preparing 1000 ml of the SBF solution

Order	Reagent	Purity (%)	Amount
1	NaCl	99.5	8.035 g
2	$NaHCO_3$	99.5	0.355 g
3	KCl	99.5	0.225 g
4	$K_2PO_4 \cdot 3H_2O$	99.0	0.231 g
5	$MgCl_2 \cdot 6H_2O$	98.0	0.311 g
6	1.0 M HCl		39 ml
7	$CaCl_2 \cdot 2H_2O$	95.0	0.388 g
8	Na_2SO_4	99.0	0.072 g
9	Tris-hydroxymethyl aminomethane	99	6.118 g
10	1.0 M HCl		0-5 ml

Fig. 1 XRD patterns of the composites (a) before and (b) after sintering at 1200 °C

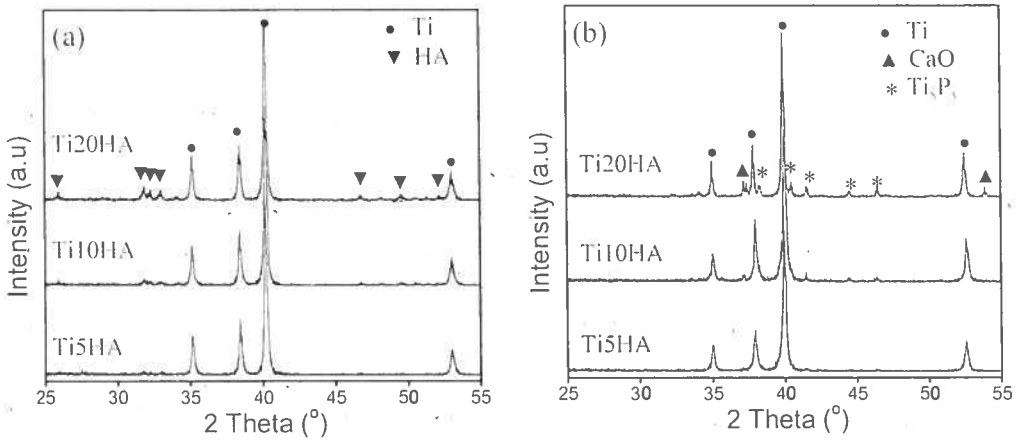

Fig. 2 The XPS survey and high resolution spectra of the composite surfaces

(a1-a4) Ti5HA; (b1-b4) Ti10HA; (c1-c4) Ti20HA

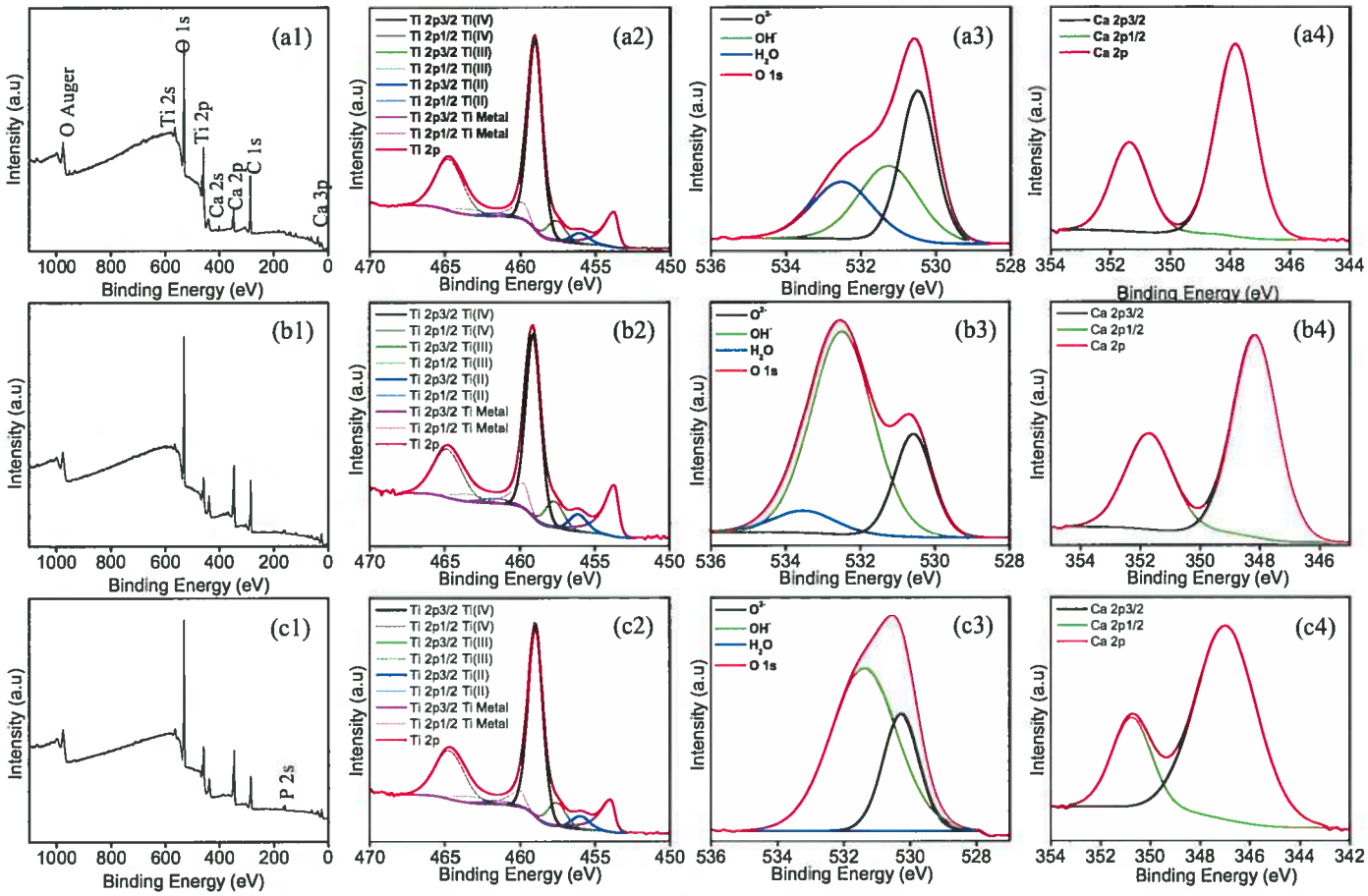

Fig. 3 Surface morphologies of the sintered Ti5HA after soaking in the SBF: (a) 0 h, (b) 8 h; (c) 1 day; (d) 3 days; (e) 7 days; (f) 14 days

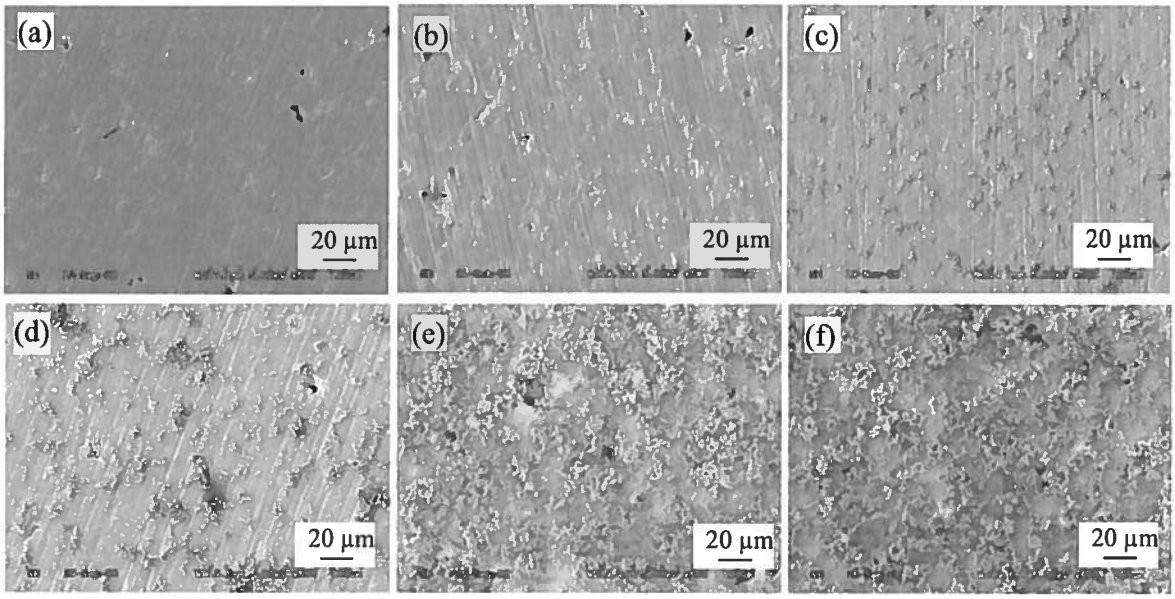

Fig. 4 Surface morphologies of the sintered Ti10 HA after soaking in the SBF: (a) 0 h, (b) 8 h; (c) 1 day; (d) 3 days; (e) 7 days; (f) 14 days

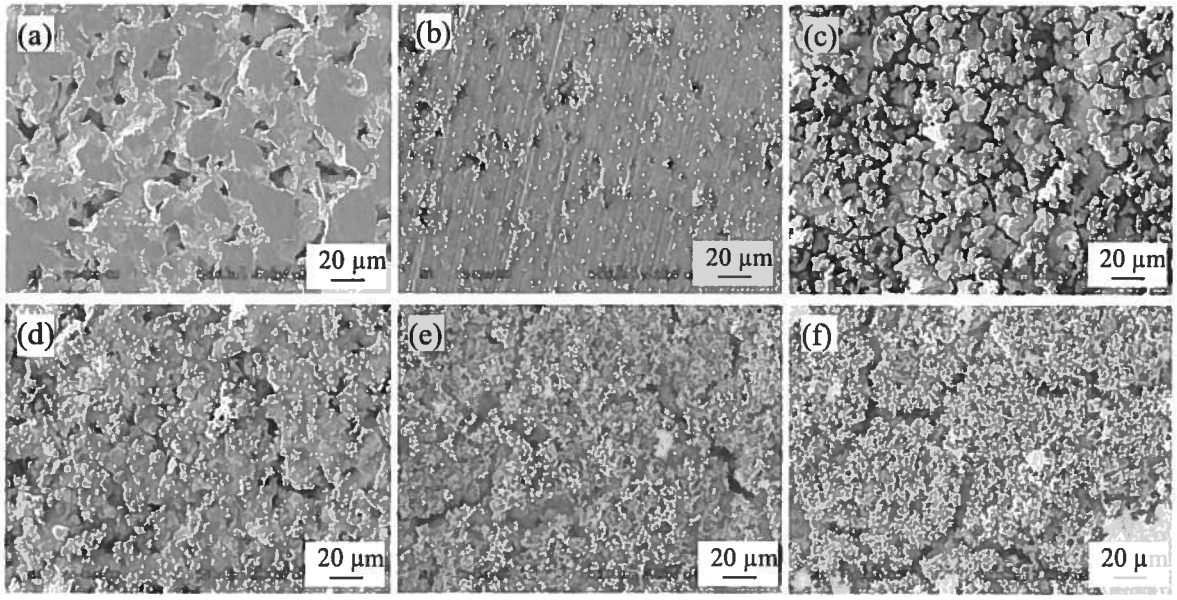

Fig. 5 Surface morphologies of the sintered Ti20HA after soaking in the SBF: (a) 0 h, (b) 8 h; (c) 1 day; (d) 3 days; (e) 7 days; (f) 14 days

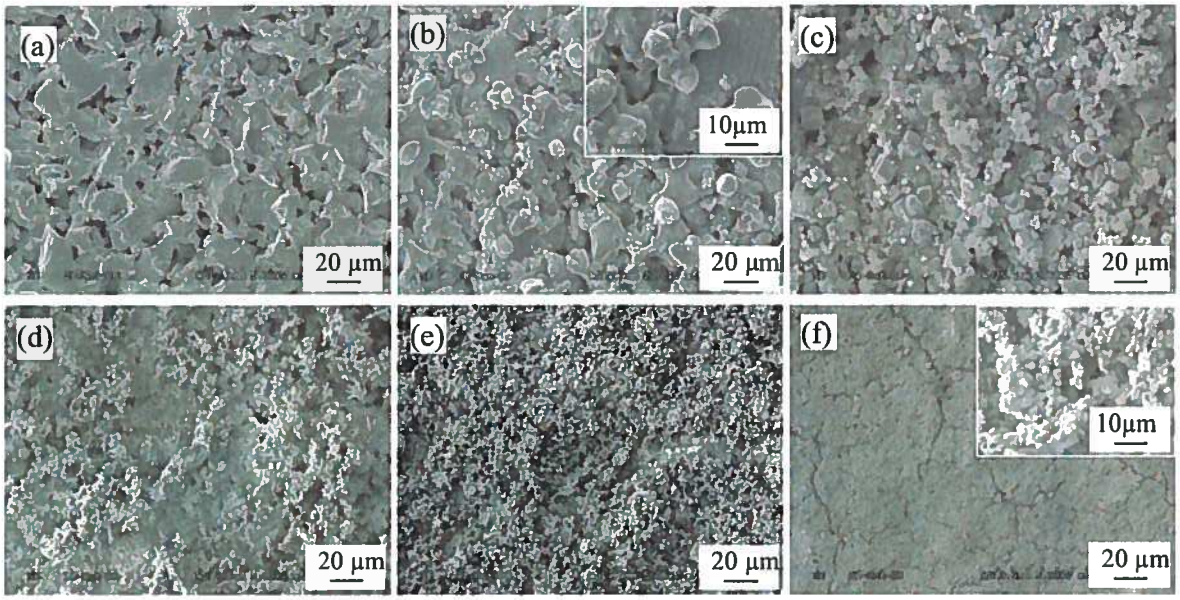

Fig. 6 EDX analysis of the SEM morphological features on Ti20HA surface after 1 day immersion in the SBF

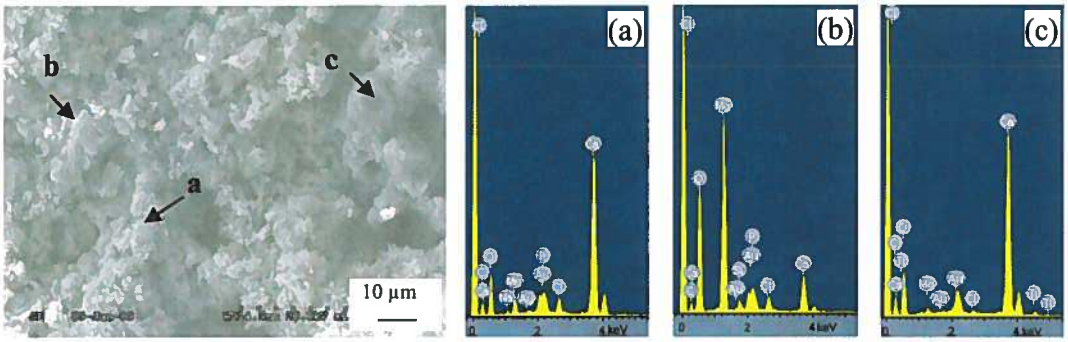

Fig. 7 FTIR of the precipitates formed on the composite surfaces after soaking in the SBF

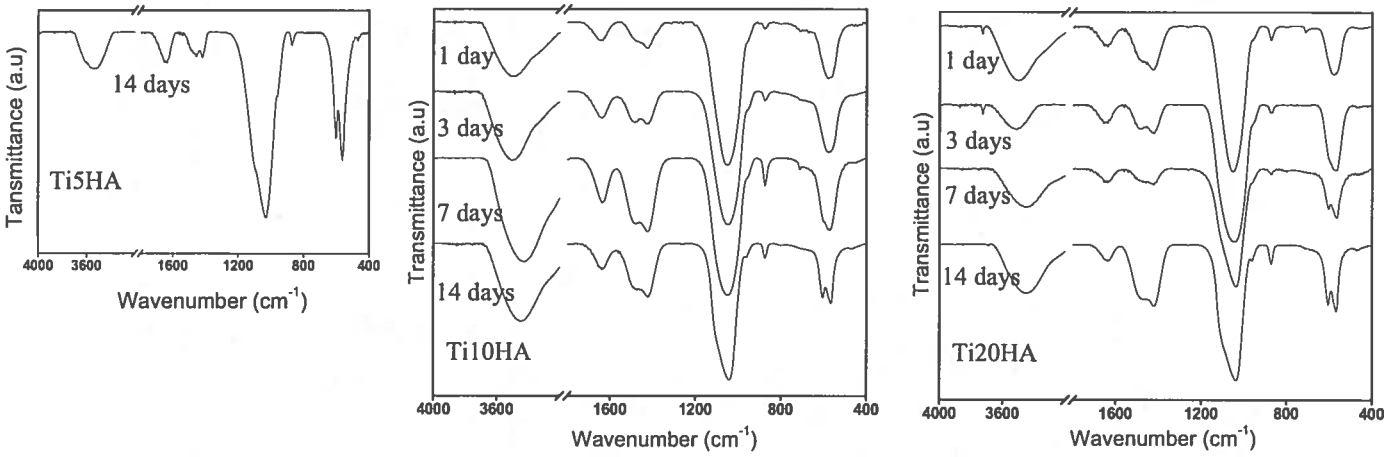

Fig. 8 Low-angle XRD patterns of the composite surface after immersion in SBF for various times: (a) Ti5HA; (b) Ti10HA; (c) Ti20HA (A: Apatite; C: $CaCO_3$; T: Ti)

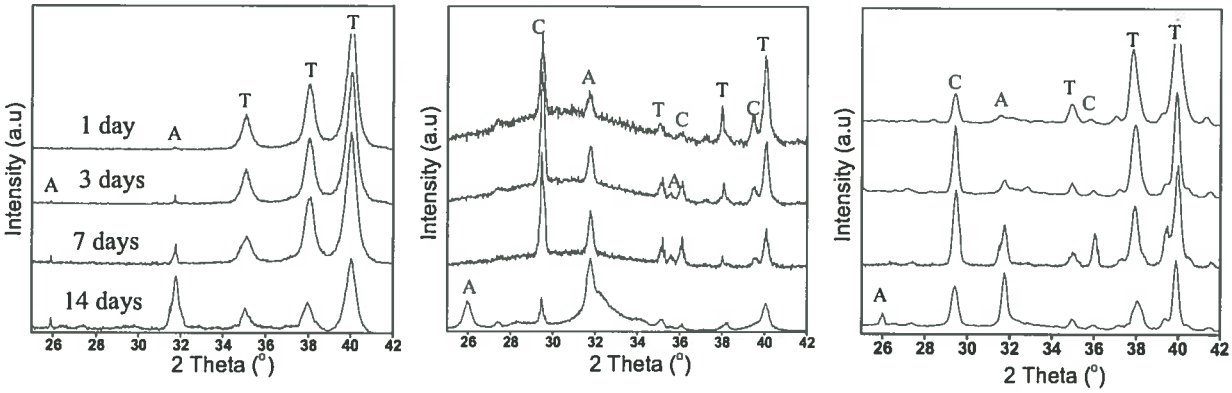

Fig. 9 pH value and ion concentrations in the SBF solution after the immersion the composites